AUT Journal of Civil Engineering

AUT J. Civil Eng., 5(4) (2021) 625-642
DOI: 10.22060/ajce.2022.19447.5732

Half-Plane Boundary Element Fundamental Solutions and Body Force

B. Ansari, A. R. Firoozfar*

Department of Civil Engineering, University of Zanjan, Zanjan, Iran.

ABSTRACT: Two-dimensional half-plane fundamental solutions have been developed by different researchers in the fields of electronics, mechanics, and geotechnics. However, for geotechnical purposes, their solutions are not complete. This paper discusses those previous solutions and details the mathematical procedures for obtaining a new and complete set of half-plane boundary element fundamental solutions. Initially, static equilibrium equations were written using Papkovitch functions and a proper Green's function was presented for a two-dimensional half-plane space. Having applied the second Green's identity, the stress-free condition for the ground surface has been satisfied in the displacement and traction fundamental solutions. These solutions can be applied in a meaningful way to problems with semi-infinite workspaces like those much seen in geophysics, geotechnical, and mining engineering because they do not need to discretize the distal boundaries of the model. After extracting half-plane fundamental solutions, the effects of the gravity force as body force and required functions for a half-plane boundary element analysis were extracted. The effectiveness and accuracy of the new solutions have been evaluated by implementing them in a boundary element computer code and solving several classic semi-infinite examples. Results showed that the new solutions are capable of accurately and economically modeling semi-infinite problems.

Review History:

Received: Jan. 03, 2021
Revised: Sep. 04, 2021
Accepted: Apr. 13, 2022
Available Online: Apr. 28, 2022

Keywords:

Half-plane
Fundamental solutions
Boundary element method
Papkovitch functions

1- Introduction

Because of their simplicity and accuracy, volumetric numerical methods such as Finite Element (FE) and Finite Difference (FD) methods are widely used for solving engineering differential equations [1, 2]. In some cases, however, conditions such as model geometry result in difficulties when volumetric methods are used, for example, in the modeling of infinite and semi-infinite domains. These problems commonly occur in many geophysical and geotechnical problems because the requirement to discretize the whole body of the model cannot be done directly in volumetric methods. The discretization of infinite and semi-infinite spaces requires artificial boundaries to close the model. What should be the distance between these artificial boundaries from the center of the model, and how large should the elements be, are two important questions for engineering analysts, as these parameters are directly proportional to the computational efforts and calculation time. To reduce the size and the number of elements, meshless approaches such as boundary integral methods have been introduced [3, 4]. In the boundary element method (BEM), which is a practical form of the boundary integral solution, discretization is only done on the boundaries of the domain. Although the boundary element technique requires fewer elements in comparison with volumetric methods, for the problems related to a semi-infinite space, it requires artificial boundaries to be again defined.

Boundary element analyses are completely based on the fundamental solutions which provide useful mathematical kernels that can be derived by satisfying the physical and boundary conditions of the problem [4, 5]. Based on those fundamental solutions and geometrical properties, the boundary element approach can be divided into Full-plane and Half-plane methods [6]. The Full-plane boundary element method is related to Kelvin's Fundamental solutions. Brebbia and Dominguez [4] described the mathematical processes required for the extraction of full-plane fundamental solutions in elasticity. Katsikadelis [5] also extracted the fundamental solutions for potential as well as elasticity problems. Brebbia and Aliabadi [7] introduced an adaptive Finite-Boundary element method for analyzing complex non-linear problems. Brebbia and Nardini [8] presented a new procedure for eigenvalue and transient dynamic analyses in solid mechanics with a boundary integral approach. More recently these methods have been successfully applied for the solution of geophysical and geotechnical problems by, Xiao and Carter [9], Panji *et al.* [10], and Panji *et al.* [11]. Another approach for solving half-space problems is the Half-plane boundary element method in which fundamental solutions

*Corresponding author's email: firoozfar@znu.ac.ir

are calculated considering the ground surface's stress-free condition.

The first attempts to satisfy the stress-free condition when extracting the solutions related to a semi-infinite elastic domain were made by Boussinesq [12] who provided the stress fundamental solutions when a point load is applied perpendicularly on the ground surface. However, these solutions cannot be used as the boundary element fundamental solutions. Cerrutti [13] obtained the displacement solutions when the point load is applied on the ground surface parallel to the stress-free boundary. In Melan's work [14] the stress fundamental solutions have been obtained when the point load is applied at an arbitrary coordinate inside a semi-infinite domain. Telles and Brebbia [15] extended Melan's work and provided the complete fundamental solutions for a boundary element analysis. However, in their traction solutions, the stress-free condition has not been completely satisfied and this causes some difficulties when modeling semi-infinite problems (Appendix B). Ye and Sawada [16] evaluated the Telles and Brebbia [15] solutions and concluded that the accuracy of the solutions decreases with increasing depth.

Fundamental solutions related to a two-dimensional semi-infinite orthotropic space were presented by Dumir and Mehta [17]. The solutions, however, are not complete and some variables have been omitted in their research so that the results cannot be used for solving practical examples. Pan et.al [18] provided a half-plane BEM formulation for anisotropic problems. But, because of non-linear procedures and using complex numbers, the implementation of these solutions for static analysis is complicated. Pan and Chen [19] provided displacement and traction solutions for static analysis of two-dimensional full-plane and half-plane problems. Their half-plane solutions are applicable when the point load is applied on the stress-free boundary (ground surface).

One of the fields that the half-plane fundamental solutions can be effectively used for reducing the calculation time are the analysis of geotechnical problems containing cavities and in-homogenous mediums. Dong and Lo [20] used the Telles and Brebbia [15] approach for the analysis of elastic half-plane domains containing Nano in-homogenous structures and showed that the half-plane solutions provided by Telles and Brebbia can be used efficiently when the problem occurs very close to the ground surface. In the three-dimensional case, Mindlin [21] provided a complete set of displacement and traction half-plane fundamental solutions.

To increase the efficiency of calculation and decrease computational time, especially for static analysis, accurate, compact, and easy-to-use half-plane solutions are required. In section 2 of this paper, the concept and importance of the half-plane fundamental solutions are clarified. In sections 3 and 4 by using the Papkovitch [22] and Green's functions [23] and applying Green's second identity [23], a new and complete set of two-dimensional half-plane boundary element fundamental solutions are obtained and the mathematical procedures are presented. Finally in section 5, by solving some classical examples, the efficiency of the new solutions is evaluated.

2- Half-Plane Boundary Element Concept

Fig. 1 shows a semi-infinite domain including three types of boundaries, Γ_1 , Γ_2 and Γ_3 , representing stress-free, far-field, and inner boundaries, respectively. For most modeling purposes including geophysical and geotechnical problems, the model space is distributed around the inner boundaries and the analytical results are important only around these types of boundaries. However, according to the full-plane analysis [4, 5], obtaining the results around the inner boundaries requires the inclusion of all other types of boundaries when discretizing and solving the model equations.

For any n-dimensional elastic space bounded by a boundary, Γ in equilibrium, displacements are related to boundary tractions with the following boundary integral equation [4, 5, and 23]:

$$c^i u^i + \int_{\Gamma=\Gamma_1\cup\Gamma_2\cup\Gamma_3} p^* u \, d\Gamma = \int_{\Gamma=\Gamma_1\cup\Gamma_2\cup\Gamma_3} u^* p \, d\Gamma \tag{1}$$

In which, u^* and p^* are the full-plane displacement and traction fundamental solutions, respectively [4] and u p are the boundary displacements and tractions. c^i is a constant related to the geometry and dimension of the problem and it is equal to 1 for internal nodes. Also, c^i can be calculated using a procedure called solid body movement when the point belongs to the boundary [4, 5, 10, 11, and 15]. Considering Fig. 1, if u^h and p^h are the half-plane fundamental solutions the boundary integral equation is modified as follows:

$$c^i u^i + \int_{\Gamma=\Gamma_3} p^h u \, d\Gamma = \int_{\Gamma=\Gamma_3} u^h p \, d\Gamma \tag{2}$$

If the u^h and p^h are the half-plane boundary element fundamental solutions; p^h and p are both equal to zero along the Γ_1 and therefore, the stress-free boundary (Γ_1) vanishes form the boundary integral equation. Since Γ_1 can be extended to infinity, the far-field boundaries (Γ_2) are also extended to infinity and the displacements and tractions along them tend to zero:

$$\lim_{r\to\infty} \int_{\Gamma_2} \left(p^h u - u^h p \right) d\Gamma = 0 \quad , \quad r : Distance \tag{3}$$

Therefore, by vanishing integrals along (Γ_1) and (Γ_2) it is only required to discretize the inner boundaries (Γ_3) when modeling a semi-infinite space.

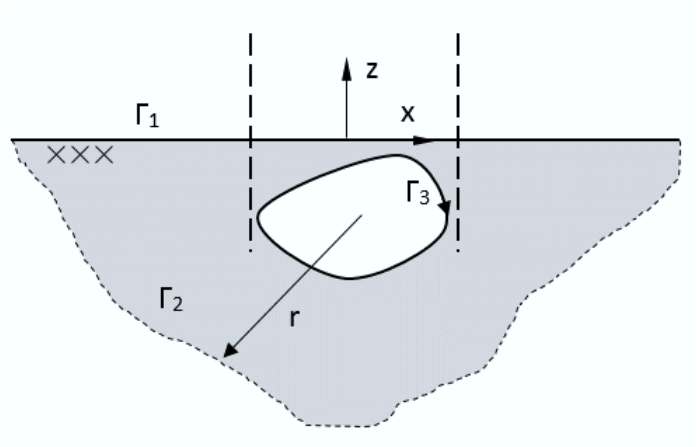

Fig. 1. Three types of boundaries related to a half-plane boundary element analysis.

3- Extracting Half-Plane Fundamental Solution ($\mathbf{u}^h$, $\mathbf{p}^h$)

For an isotropic elastic body in equilibrium the displacement can be expressed by the following equation [4, 5] (bold letters are used for vectors and tensors):

$$\mu\nabla^2\boldsymbol{u}+\frac{\mu}{1-2\nu}\nabla\nabla\boldsymbol{u}+\boldsymbol{F}=0 \tag{4}$$

In which μ and ν are the shear modulus and Poisson's ratio, respectively, and $\boldsymbol{F}$ is the body force per unit volume. In this equation ∇ is the gradient vector and can be defined as $\nabla=\left(\partial/\partial x,\ \partial/\partial y,\ \partial/\partial z,\ldots\right).\nabla$ and ∇^2 are the n-dimensional gradient and Laplace operators, respectively.

Using Hooke's laws the stresses can be calculated from displacement as follows [4, 5]:

$$\boldsymbol{\sigma}=\lambda\nabla\boldsymbol{u}\boldsymbol{I}+\mu\left(\nabla^{\mathrm{T}}\boldsymbol{u}+\boldsymbol{u}^{\boldsymbol{T}}\nabla\right) \tag{5}$$

Where $\lambda=2\mu\nu/1-2\nu$ is the Lame's constant and $\boldsymbol{I}$ is the unit matrix.

By using Eq. (4), it can be shown that the displacement vector can be decomposed into a scalar field β and a vector field $\boldsymbol{B}$ as follows:

$$\boldsymbol{u}=M\left(\boldsymbol{B}\right)+N\left(\beta\right) \tag{6}$$

In which M and N are two linear operators. Considering two potential functions $\boldsymbol{H}$ and φ, Helmholtz's theorem [22] can be used for decomposing the displacement vector:

$$\boldsymbol{u}=\nabla\varphi+\nabla\times\boldsymbol{H}\ and\ \nabla.\boldsymbol{H}=0 \tag{7}$$

Substituting into the equilibrium equation (Eq. (4)):

$$\mu\nabla^2\left(\frac{2\left(1-\nu\right)}{1-2\nu}\nabla\varphi+\nabla\times\boldsymbol{H}\right)+\boldsymbol{F}=0 \tag{8}$$

Defining the Papkovitch vector function, $\boldsymbol{B}=(2\left(1-\nu\right)/1-2\nu)\nabla\varphi+\nabla\times\boldsymbol{H}$:

$$\mu\nabla^2\boldsymbol{B}=-\boldsymbol{F} \tag{9}$$

Hence:

$$\frac{2\left(1-\nu\right)}{1-2\nu}\nabla^2\varphi=\nabla.\boldsymbol{B} \tag{10}$$

One special solution for the above differential equation can be obtained as follows:

$$\frac{4\left(1-\nu\right)}{1-2\nu}\varphi=\boldsymbol{r}.\boldsymbol{B}+\beta \tag{11}$$

In which β is the Papkovitch scalar function with the following relation:

$$\mu\nabla^2\beta = \boldsymbol{r}.\boldsymbol{F} \quad and \quad \boldsymbol{r} = x\boldsymbol{i} + y\boldsymbol{j} \tag{12}$$

By substituting Eq. (11) into Eq. (7) with considering the fact that $\nabla\times\boldsymbol{H} = \boldsymbol{B} - (2(1-\nu)/1-2\nu)\nabla\varphi$:

$$\boldsymbol{u} = \boldsymbol{B} - \frac{1}{4(1-\nu)}\nabla(\boldsymbol{r}.\boldsymbol{B} + \beta) \tag{13}$$

With $M(\boldsymbol{s}) = \boldsymbol{s} - (1/4(1-\nu))\nabla(\boldsymbol{r}.\boldsymbol{s})$ and $N(s) = -(1/4(1-\nu))\nabla(s)$.

Considering a scalar potential function V distributed in an n-dimensional space Ω bounded by Γ, the Green's second identity can be defined as follows [23]:

$$KV = \int_\Gamma V\ \frac{\partial G}{\partial \boldsymbol{n}}d\Gamma + \int_\Omega G\ \nabla^2 V\ d\Omega \tag{14}$$

in which G is the half-plane Green's function, K shows a constant related to the dimension of the problem and $\boldsymbol{n}$ is the normal outward vector to the boundary. For a two-dimensional space a half-plane Green's function concerning $z = 0$ that satisfies the Laplace equation $(\nabla^2 G = 0)$ can be defined as follows:

$$G = \ln\sqrt{(x-\alpha)^2 + (z-\beta)^2} - \ln\sqrt{(x-\alpha)^2 + (z+\beta)^2} = \ln r - \ln r' \tag{15}$$

In which r is the distance of a source point (α, β) from a field point (x, z) and r' stands for the image r concerning the boundary, $z = 0$.

Fundamental solutions Part 1: To obtain half-plane fundamental solutions, at first we assumed that a concentrated load is applied at a point $(\alpha = 0, \beta = c)$ in the direction of the z-axis. Therefore all components of load along both the x-axis and the y-axis are equal to zero. Considering Eq. (5) and applying $B_x = B_y = 0$ and $F_x = F_y = 0$, the tractions on the stress-free boundary $(z = 0)$ can be expressed as follows:

$$\sigma_{zz} = \frac{\mu}{2(1-\nu)}\left[2(1-\nu)\frac{\partial B_z}{\partial z} - \frac{\partial^2\beta}{\partial z^2}\right] = 0\ on\ z = 0 \tag{16}$$

$$\sigma_{zx} = \frac{\mu}{2(1-\nu)}\left[(1-2\nu)\frac{\partial B_z}{\partial x} - \frac{\partial^2\beta}{\partial x\,\partial z}\right] = 0 on\ z = 0 \tag{17}$$

By integrating the latter equation with respect to x and applying the Laplace operator, then using Green's second identity $z \neq 0$, the following equations can be obtained:

$$\nabla^2\left(\left[(1-2\nu)B_z - \frac{\partial\beta}{\partial z}\right]\right) = (1-2\nu)\nabla^2 B_z - \frac{\partial\nabla^2\beta}{\partial z} = -\frac{(1-2\nu)}{\mu}F_z - \frac{1}{\mu}\frac{\partial(zF_z)}{\partial z} \tag{18}$$

$$K\left[(1-2\nu)B_z - \frac{\partial\beta}{\partial z}\right] = -\frac{1}{\mu}\int\left[(1-2\nu)GF_z + G\frac{\partial(\beta F_z)}{\partial\beta}\right]d\Omega \tag{19}$$

In the above equation, the boundary term of Green's second identity vanishes because of the stress-free condition along, $z = 0$. The first part of the integral when the point load is of a form $F_z = P_z\delta(\alpha)\delta(\beta - c)$ can be obtained as follows:

$$\int_\Omega (1-2\nu)GP_z\delta(\alpha)\delta(\beta-c)d\Omega = (1-2\nu)(\ln r - \ln r')P_z \tag{20}$$

In which P_z is the constant magnitude of the point load (Fig. 2) and δ is the Dirac delta function. The second part of the integral can be taken by parts as follows:

$$\int_\Omega G\frac{\partial(\beta F_z)}{\partial\beta}d\Omega = -\int_\Omega \frac{\partial G}{\partial\beta}\beta P_z\delta(\alpha)\delta(\beta-c)\,d\Omega = -cP_z\frac{\partial G}{\partial\beta} = cP_z\frac{\partial}{\partial z}(\ln r + \ln r') \tag{21}$$

In which again the boundary integral vanished because of the half-plane Green's function. Substituting Eqs. (20) and (21) into the (19) for $z \neq 0$:

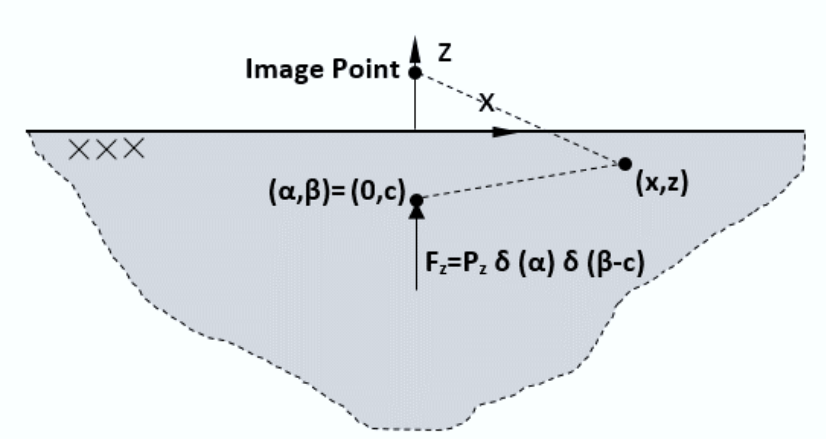

Fig. 2. Point load acted in the direction of the z-axis.

$$\left(1-2\nu\right)B_z-\frac{\partial\beta}{\partial z}= -\frac{P_z}{\mu K}\left[\left(1-2\nu\right)\left(\ln r-\ln r'\right)+c\frac{\partial}{\partial z}\left(\ln r+\ln r'\right)\right] \quad (22)$$

Again considering Eq. (5) and following the same procedures as discussed above for $z\neq 0$ one can obtain:

$$2\left(1-\nu\right)B_z-\frac{\partial\beta}{\partial z}= -\frac{P_z}{\mu K}\left[2\left(1-\nu\right)\left(\ln r+\ln r'\right)+c\frac{\partial}{\partial z}\left(\ln r-\ln r'\right)\right] \quad (23)$$

Eqs. (10) and (11) present two linear differential equations that can be solved analytically to obtain B_z β:

$$B_z=-\frac{P_z}{\mu K}\left[\ln r+\left(3-4\nu\right)\ln r'-2c\frac{\partial}{\partial z}\left(\ln r'\right)\right] \quad (24)$$

$$\beta=\frac{P_z}{\mu K}\left[-4\left(1-\nu\right)\left(1-2\nu\right)\int\ln r'dz+ c\left(\ln r+\left(3-4\nu\right)\ln r'\right)\right] \quad (25)$$

Now it is possible to use the result of Eq. (13) to obtain displacement fundamental solutions when the load acts in the direction of the z-axis as follows:

$$U_{21}=-\frac{1}{4\left(1-\nu\right)}\left[zA_1\left(x,z\right)+A_2\left(x,z\right)\right] \quad (26)$$

$$U_{22}=\frac{1}{4\left(1-\nu\right)}\times \left[\left(3-4\nu\right)A_3\left(x,z\right)-zA_4\left(x,z\right)-A_5\left(x,z\right)\right] \quad (27)$$

In which, $A_i\left(x,z\right)$ are the functions that are presented in Appendix A.

Using displacement components U_{21} and U_{22} and Eq. (5), the components of the stress tensor can be obtained as follows:

$$\sigma_{112}=\frac{1}{2\left(1-\nu\right)}\times \left\{\lambda\left(1-2\nu\right)A_4\left(x,z\right)-\mu\left(zA_6\left(x,z\right)+A_7\left(x,z\right)\right)\right\} \quad (28)$$

$$\sigma_{122}=\sigma_{212}=\frac{\mu}{2\left(1-\nu\right)}\times \left\{\left(1-2\nu\right)A_1\left(x,z\right)-zA_8\left(x,z\right)-A_9\left(x,z\right)\right\} \quad (29)$$

$$\sigma_{222}=\frac{1}{2(1-\nu)}\times \left\{(\lambda+2\mu)(1-2\nu)A_4(x,z)+\mu\left(zA_6(x,z)+A_7(x,z)\right)\right\} \tag{30}$$

Finally, the tractions along the boundaries can be calculated by multiplying the stress tensor into the unit normal vector to the boundary.

Fundamental solutions part 2: In the second part we considered a concentrated load acting at a point $(\alpha=0,\beta=c)$ in the direction of the x-axis (Fig. 3). Using Eq. (5) and applying $F_z=F_y=0$ and $B_y=0$ the following conditions can be obtained along, $z=0$:

$$\sigma_{zz}=\frac{\mu}{2(1-\nu)}\times \left[\frac{a_1}{2}\left(\frac{\partial B_z}{\partial x}+\frac{\partial B_x}{\partial z}\right)-x\frac{\partial^2 B_x}{\partial z\,\partial x}-\frac{\partial^2\beta}{\partial z\,\partial x}\right]=0 on\ z=0 \tag{31}$$

$$\sigma_{zx}=\frac{\mu}{2(1-\nu)}\times \left[a_2\frac{\partial B_x}{\partial x}+a_3\frac{\partial B_z}{\partial z}-x\frac{\partial^2 B_x}{\partial z^2}-\frac{\partial^2\beta}{\partial z^2}\right]=0 on\ z=0 \tag{32}$$

Where $a_1=2(1-2\nu)$, $a_2=\lambda a_1/2\mu$ and $a_3=(\lambda+2\mu)a_1/2\mu$. These equations present two differential equations with three unknown functions B_x, B_z, and β. Considering Eq. (3), B_x can be calculated as follows:

$$B_x=-\frac{P_x}{\mu K}\left(\ln r+\ln r'\right) \tag{33}$$

Since $\frac{\partial B_x}{\partial z}|_{z=0}$ and $\frac{\partial^2 B_x}{\partial z\,\partial x}|_{z=0}$ are both equal to zero along, $z=0$; from the Eq. (31) one can obtain:

$$\frac{a_1}{2}B_z-\frac{\partial\beta}{\partial z}=0 on\ z=0 \tag{34}$$

Considering Eq. (32) on $z=0$, the following equation is always valid:

$$a_2\frac{\partial B_x}{\partial x}-x\frac{\partial^2 B_x}{\partial z^2}=(a_2-1)\frac{\partial B_x}{\partial x}+\frac{2P_x c}{\mu K}\frac{\partial^2(\ln r')}{\partial z\,\partial x} \tag{35}$$

Hence:

$$a_3\frac{\partial B_z}{\partial z}-\frac{\partial^2\beta}{\partial z^2}+(a_2-1)\frac{\partial B_x}{\partial x}+\frac{2P_x c}{\mu K}\frac{\partial^2(\ln r')}{\partial z\,\partial x}=0\ on\ z=0 \tag{36}$$

Applying Green's second identity on Eqs. (35) and (36) for $z\neq 0$:

$$\frac{a_1}{2}B_z-\frac{\partial\beta}{\partial z}=0 on\ z\neq 0 \tag{37}$$

$$a_3B_z-\frac{\partial\beta}{\partial z}=\frac{2P_x}{\mu K}\left[-\frac{cx}{r'^2}+(a_2-1)\tan^{-1}\left(\frac{z+c}{x}\right)\right] on\ z\neq 0 \tag{38}$$

These two equations present two linear differential equations that can be solved to obtain unknowns B_z and β as follows:

$$B_z=\frac{2P_x}{\mu K}\left[-\frac{cx}{r'^2}+(a_2-1)\tan^{-1}\left(\frac{z+c}{x}\right)\right] \tag{39}$$

$$\beta=\frac{a_1P_x}{\mu K}\times \left[-c\tan^{-1}\left(\frac{z+c}{x}\right)+(a_2-1)\int\tan^{-1}\left(\frac{z+c}{x}\right)dz\right] \tag{40}$$

By using the result of Eq. (13), the displacement fundamental solutions when the point load acts in the direction of the x-axis can be calculated as follows:

$$U_{11}=\frac{1}{4(1-\nu)}\times \left[(3-4\nu)B_1(x,z)-(x-\alpha)B_2(x,z)-zB_3(x,z)-B_4(x,z)\right] \tag{41}$$

$$U_{12}=\frac{1}{4(1-\nu)}\times \left[(3-4\nu)B_5(x,z)-(x-\alpha)B_6(x,z)-zB_7(x,z)-B_8(x,z)\right] \tag{42}$$

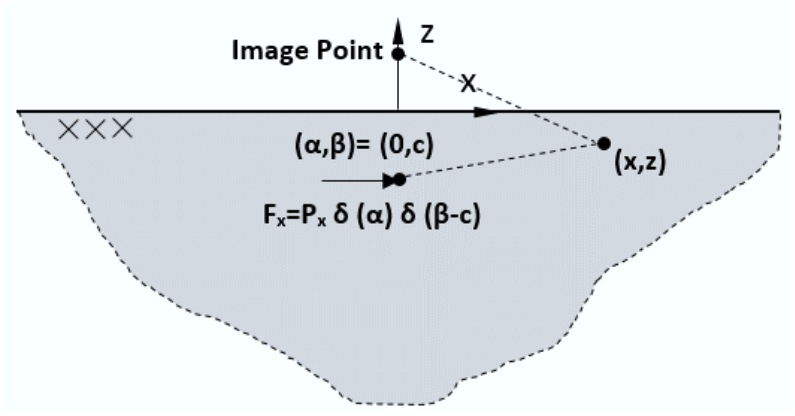

Fig. 3. Point load acted in the direction of the x-axis.

In which $B_i(x,z)$ are the functions represented in Appendix A.

Similar to the previous part (load along the z-axis), traction fundamental solutions can be extracted from the stress tensor components considering Eq. (5) as follows:

$$\sigma_{111}=\frac{1}{4(1-\nu)}\times \begin{Bmatrix} a_1\left((\lambda+2\mu)B_2(x,z)+\lambda B_7(x,z)\right) \\ -2\mu\left((x-\alpha)B_9(x,z)+zB_{10}(x,z)+B_{11}(x,z)\right) \end{Bmatrix} \quad (43)$$

$$\sigma_{121}=\sigma_{211}=\frac{\mu}{2(1-\nu)}\times \begin{Bmatrix} (1-2\nu)\left(B_3(x,z)+B_6(x,z)\right) \\ -(x-\alpha)B_{12}(x,z)-zB_{13}(x,z)-B_{14}(x,z) \end{Bmatrix} \quad (44)$$

$$\sigma_{221}=\frac{1}{4(1-\nu)}\times \begin{Bmatrix} a_1\left(\lambda B_2(x,z)+(\lambda+2\mu)B_7(x,z)\right) \\ +2\mu\left((x-\alpha)B_9(x,z)+zB_{10}(x,z)+B_{11}(x,z)\right) \end{Bmatrix} \quad (45)$$

Calculation of K constant: As discussed previously, K is a dimension-related constant. Weatherburn [23] showed that in the case of three-dimensional space, K is equal to -4π. For a half-plane two-dimensional case, it is possible to calculate K by applying Green's second identity and using half-plane Green's function. Fig. 4 shows a semi-infinite space subjected to concentrated load acted in a point (α,β) surrounded by a circular boundary with a radius of ε. Applying Green's second identity:

$$\int_{\Gamma_1}\left(G\frac{\partial V}{\partial \boldsymbol{n}}-V\frac{\partial G}{\partial \boldsymbol{n}}\right)d\Gamma_1 = \int_{\Gamma_2}V\frac{\partial G}{\partial \boldsymbol{n}}d\Gamma_2+\int_{\Omega}G\nabla^2V\,d\Omega \quad (46)$$

On the boundary of the surrounding circle when ε tends to zero:

$$\int_{\Gamma_1}G\frac{\partial V}{\partial \boldsymbol{n}}d\Gamma_1 = \lim_{\varepsilon\to 0}\left(\ln\varepsilon-\ln\varepsilon'\right)\times 2\pi\varepsilon\times\frac{\partial V}{\partial \boldsymbol{n}}=0 \quad (47)$$

And

$$-\int_{\Gamma_1}V\frac{\partial G}{\partial \boldsymbol{n}}d\Gamma_1 = -\lim_{\varepsilon\to 0}\left(-\frac{1}{\varepsilon}+\frac{\partial\ln\varepsilon'}{\partial\varepsilon}\right)\times 2\pi\varepsilon=2\pi V \quad (48)$$

Therefore, K is equal to 2π.

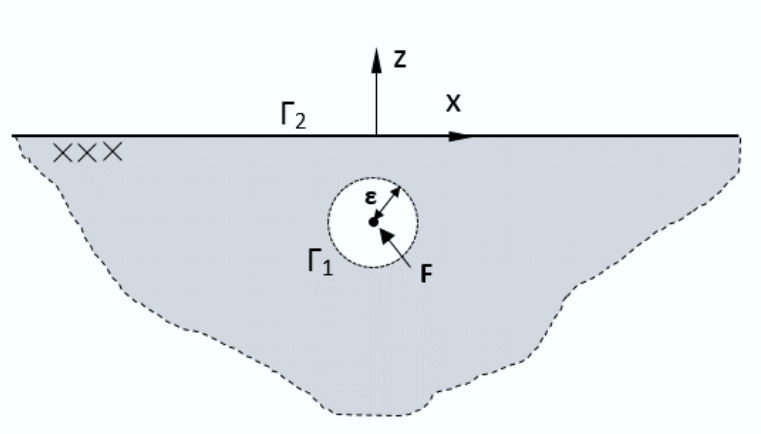

Fig. 4. Point load surrounded by a circle.

4- Half-space Body Force

A body force is a force that acts throughout the volume of the body. Gravity, electric force, and magnetic force can be considered as the body forces when modeling static and dynamic problems. For most mechanical and geotechnical purposes the body force due to gravity is most important. In general, the force of gravity is not a constant value and it can vary as a function of space and time. However, for a small area on the earth's surface, the variation of the force is so small that can be considered a constant value.

For a half-space problem considering gravity force in the solution, needs to model far-field boundaries and discretize the whole volume of the body which requires heavy computational efforts and calculation time even for a constant value of the body force. Body force can be considered in the solution as the integral of the force per unit volume along the whole volume of the body as follows:

$$B_i = \int_\Omega u_{ij}^h b_j \, d\Omega \tag{49}$$

In which b_j is the j th component of body force per unit volume and u_{ij}^h is the half-plane displacement fundamental solution extracted in the previous section. Considering a constant force in each direction, the above domain integral can be converted into the half-plane boundary integral as follows:

$$\int_\Omega u_{ij}^h b_j \, d\Omega = \int_{\Gamma_3} p_{ij}^h \Psi_j \, d\Gamma_3 - \int_{\Gamma_3} u_{ij}^h \eta_j \, d\Gamma_3 + c_{ij} \Psi_j (\alpha, \beta) \tag{50}$$

Where p_{ij}^h, is the half-plane traction fundamental solution extracted in the previous section, and (α, β) is the coordinate of the source point. c_{ij}, are the geometry-related constant that can be calculated using a method called solid body movement [4]. Ψ_j and η_j are the known functions that were extracted as follows:

$$\Psi_1 = \frac{b_x}{2\mu S} x^2$$

$$\Psi_2 = -\frac{\lambda b_x}{(\lambda+2\mu)\mu S} xz + \frac{(1-2\nu) b_z}{4\mu(1-\nu)} z^2$$

$$\eta_1 = \frac{b_x}{\mu S}\left\{\left[(\lambda+2\mu) - \frac{\lambda^2}{(\lambda+2\mu)}\right] x n_1 - \frac{\lambda\mu}{(\lambda+2\mu)} z n_2\right\} + \frac{b_z (1-2\nu)\lambda}{2\mu(1-\nu)} z n_1 \tag{51}$$

$$\eta_2 = -\frac{b_x \lambda}{(\lambda+2\mu) S} z n_1 + \frac{b_z (1-2\nu)(\lambda+2\mu)}{2\mu(1-\nu)} z n_2$$

In which b_x and b_z are the components of the constant body force per unit volume in the direction of x and z axis, respectively. n_j is the j th component of the unit normal vector to the boundary and S is constant that can be calculated as follows:

$$S = 1 + \frac{2\mu}{(1-2\nu)(\lambda+2\mu)} \tag{52}$$

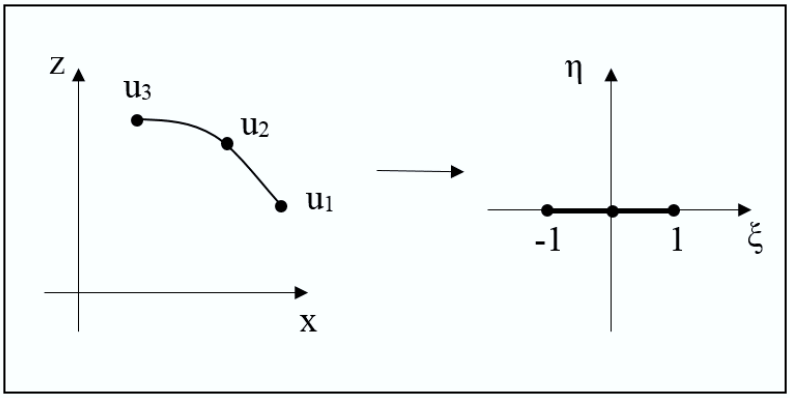

Fig. 5. Transferring the coordinate of the model space to the unit space.

5- Boundary Integral Equation and Discretization:

Fundamental solutions derived in section 3, provide a second-order tensor with the following components [4, 5]:

$$u^h = \begin{bmatrix} U_{11} & U_{12} \\ U_{21} & U_{22} \end{bmatrix} \tag{53}$$

Similarly, traction fundamental solutions can be calculated from stress tensors as follows [4, 5]:

$$p_{ij}^h = \sigma_{jki} n_k \tag{54}$$

In which p_{ij}^h are the components of the traction fundamental solutions tensor and σ_{jki} are the stress components which were presented in the previous section. n_k is the k th component of the unit vector normal to the boundary. The half-plane boundary integral equation by applying the half-plane fundamental solutions and half-plane body forces into the equilibrium equation can be expressed as follows:

$$\begin{aligned} &c_{ij} u_j(\alpha,\beta) + \int_{\Gamma_3} p_{ij}^h u_j \, d\Gamma_3 = \\ &\int_{\Gamma_3} u_{ij}^h p_j \, d\Gamma_3 + \int_{\Gamma_3} p_{ij}^h \Psi_j \, d\Gamma_3 - \\ &\int_{\Gamma_3} u_{ij}^h \eta_j \, d\Gamma_3 + c_{ij} \Psi_j(\alpha,\beta) \end{aligned} \tag{55}$$

According to Fig. 1, Eq. (55) shows that the calculation of the displacement field u_j only requires discretizing the inner boundaries, Γ_3. The discretized form of the equation can be presented as follows:

$$HU = GP + H\Psi - G\eta \tag{56}$$

In which H and G are the discretized form of the fundamental solutions. By considering the NE number of boundary elements the integrals can be expressed as follows:

$$\begin{aligned} H &= \sum_{n=1}^{NE} \int_{\Gamma_n} p_{ij}^h \varphi d\Gamma_n \\ G &= \sum_{n=1}^{NE} \int_{\Gamma_n} u_{ij}^h \varphi d\Gamma_n \end{aligned} \tag{57}$$

According to Fig. 5, for a quadratic element the shape function, φ, can be extracted by using the properties of the unit space as follows [4]:

$$\varphi = \begin{bmatrix} \frac{\xi}{2}(\xi-1) & 0 & 1-\xi^2 & 0 & \frac{\xi}{2}(\xi+1) & 0 \\ 0 & \frac{\xi}{2}(\xi-1) & 0 & 1-\xi^2 & 0 & \frac{\xi}{2}(\xi+1) \end{bmatrix} \tag{58}$$

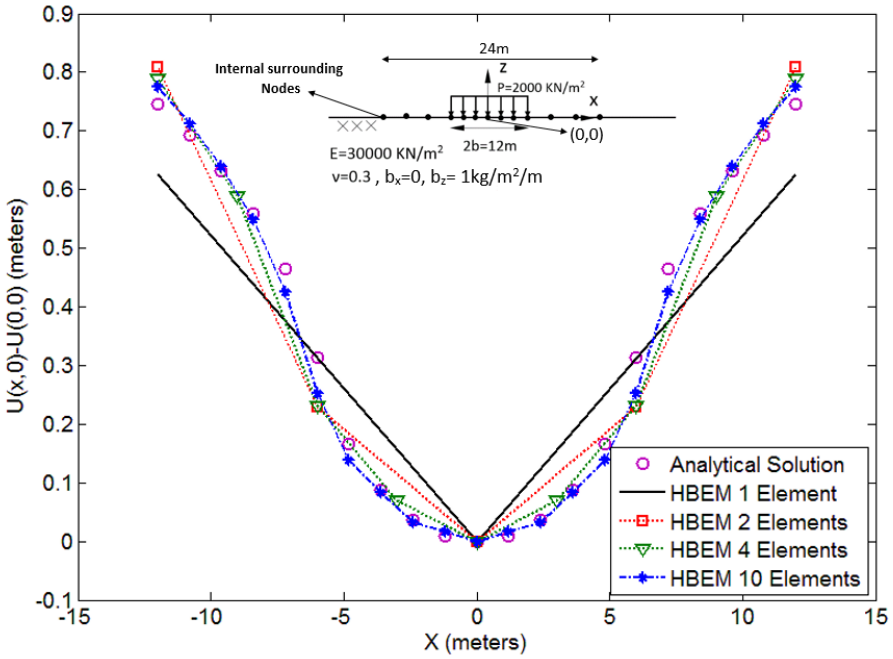

Fig. 6. Vertical displacement due to the vertical traction acted on the surface of a semi-infinite space.

Some expressions in the fundamental solutions contain $\tan^{-1}(a/b)$ function (see for example expression $A_2(x,z)$ in Appendix A). Most computer algorithms compute $\tan^{-1}(a/b)$ as zero when the "a" value tends to zero. However, for a boundary element analysis the sign of "b" is important. For modifying $\tan^{-1}(-)$ function following algorithm is suggested:

$$\begin{cases} \tan^{-1}\left(\dfrac{0}{b}\right)=0 \quad if\ b>0 \\ \tan^{-1}\left(\dfrac{0}{b}\right)=\pi \quad if\ b<0 \end{cases} \tag{59}$$

The formulation and boundary element fundamental solutions provided in this section, do not make any special difficulties when applying to the boundary integral Eq. (55) and all singularities are the same as traditional boundary element methods [4, 5]. The main difference between the presented half-plane method and traditional BEM formulations is the discretization process. In half-plane formulation, only the boundaries of the cavities and topographic reliefs are discretized and it is not necessary to define the far-field boundaries to close the model. Therefore, the number of boundary elements required to calculate the responses is significantly reduced resulting in much lesser computational efforts to solve the model. The only limitation of the new method is the uniqueness problem as described by Telles and Brebbia [15]. This problem appears when the boundaries of the model are not closed-form the sides. In this situation, the results of the solution are differential deformations. When the deformation is initialized for only one point of the domain is possible to convert all differential deformations to real deformations in the model. Therefore the uniqueness problem won't make any special difficulties for the BEM analysis and different methods have been developed for solving the problem [15].

6- Numerical Examples

Half-plane under surface loading: In the first example three kinds of linear distribution of traction over a finite part of a semi-infinite plane were evaluated. The problem was solved by only discretizing the loaded part of the surface using quadratic boundary elements and the results for surface displacement were computed using a Matlab code solution at boundary nodes. The analytical solution for this example is available in Poulos and Davis [25].

The first case is related to a strip vertical loading acting in the direction of the z-axis (Fig. 6). As Poulos and Davis [25] described, the vertical displacement of the ground surface nodes can be calculated analytically by the following equation:

$$u_z(x,0)-u_z(0,0)=\frac{2p(1-\nu^2)}{\pi E}\times \\ \left\{(x-b)\ln|x-b|-(x+b)\ln|x+b|+2b\ln b\right\} \tag{60}$$

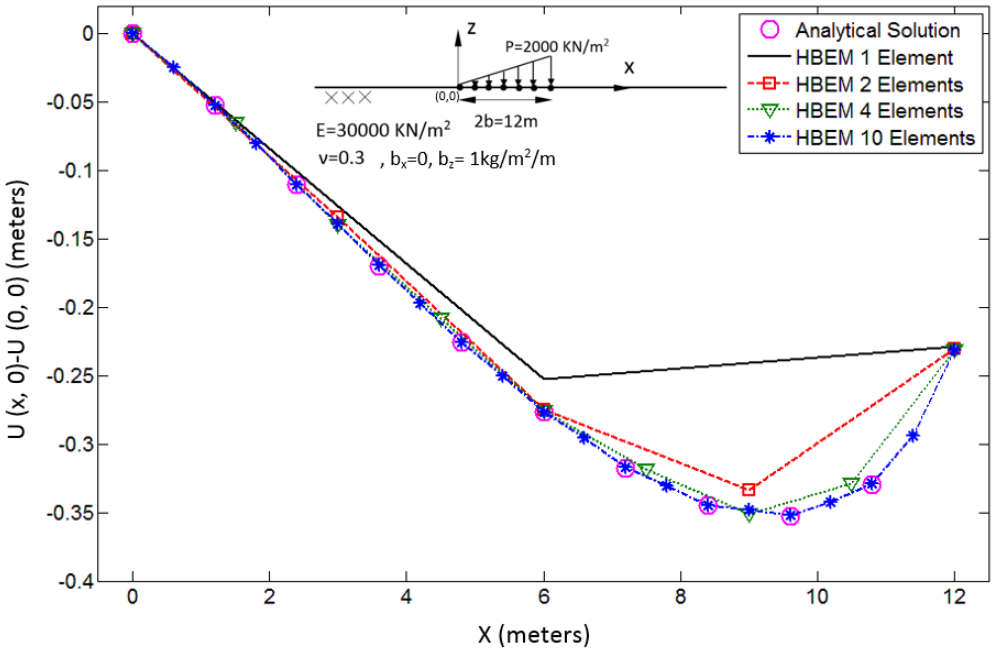

Fig. 7. Vertical displacement due to the vertical triangle traction acted on the surface of a semi-infinite space.

In which $u_z(x,0)$ is the vertical displacement at any point on the surface and $u_z(0,0)$ is the vertical displacement at the center of the loading. p is the magnitude of loading, b is the half-length of the loading line and ν and E are the Poisson's ratio and Elastic modulus of the domain, respectively. Fig. 6 shows the comparison between analytical and half-plane boundary element solutions. For clarifying the robustness of the method, the deformation results are plotted in the nodes under the loading area and also for the surrounding points. According to Fig. 6, the loading width is 12m and the results are calculated for 24m. As can be seen in the figure, there is a good agreement between the two sets of solutions and it indicates that the displacement part of the fundamental solutions works correctly in the case of surface loading.

In the second test, a linear surface loading is considered. According to Poulos and Davis [25], the vertical displacement due to normal triangle traction acting on the surface can be obtained as follows:

$$u_z(x,0)-u_z(0,0)=\frac{p(1-\nu^2)}{\pi bE}\times \left\{2b^2\ln 2b-\frac{x^2}{2}\ln x+\left(\frac{x^2}{2}-2b^2\right)\ln|2b-x|+bx\right\} \quad (61)$$

In which p is the maximum magnitude of the linear loading. Fig. 7 shows the results of analytical and numerical solutions. A proper agreement can be seen between the results.

Shallow Circular Cavity under Pressure: The second verification example presents a circular cavity embedded in a semi-infinite space (Fig. 8). A uniform pressure with a magnitude of $100\,KPa$ is applied over the internal boundary of the cavity. The ratio between cavity embedded depth and radius is equal to $d/r=1.34$ and the material properties of the domain are the same as in previous examples. The stress distribution in an element inside the domain of this problem can be calculated using the computed displacements. To reach this goal, there are several approaches proposed by Liu and Jeffers [26, 27] and Liu [28]. For example, Liu and Jeffers [26] introduced a new method for discretizing the model domain by rational triangular Bézier splines. By defining a nine-node internal element and calculating the vertical and horizontal displacements in the nodes, the displacement function can be estimated by a Lagrange interpolation or spline functions [28, 29]. The function then can be differentiated concerning x and z and finally the stress components can be calculated using Eq. (5). In Fig. 9 the computed numerical results were compared to an analytical solution obtained by Jeffry [30]. As can be seen, there is a good agreement between the two solutions.

Ground surface vertical displacement and horizontal stresses due to internal pressure of shallow cavities embedded in different depths of the soil are provided in Fig. 10. It can be seen that by increasing the depth of the cavity, both horizontal stress and vertical displacement decrease. The deformed shapes of the cavity are presented

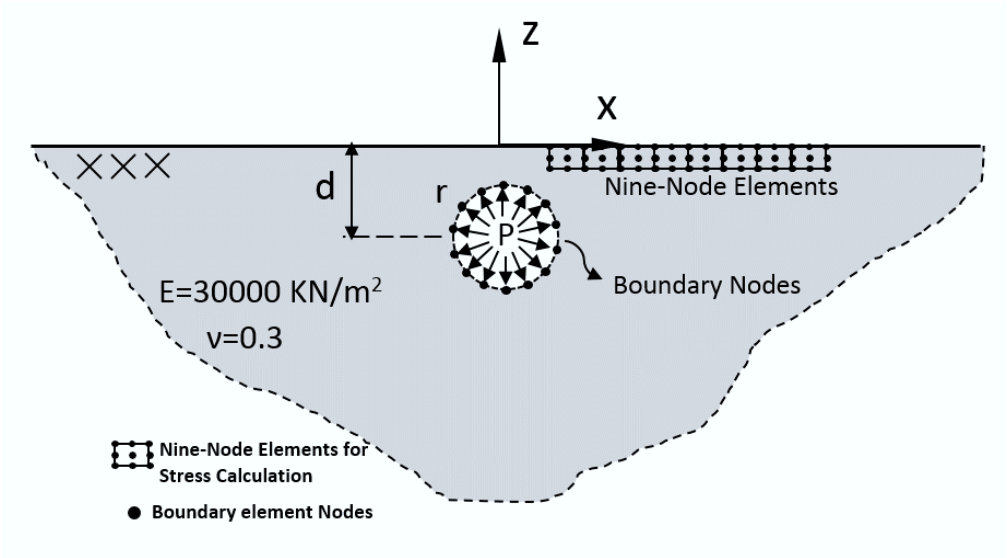

Fig. 8. Schematic representation of a shallow circular cavity under pressure embedded in a semi-infinite space.

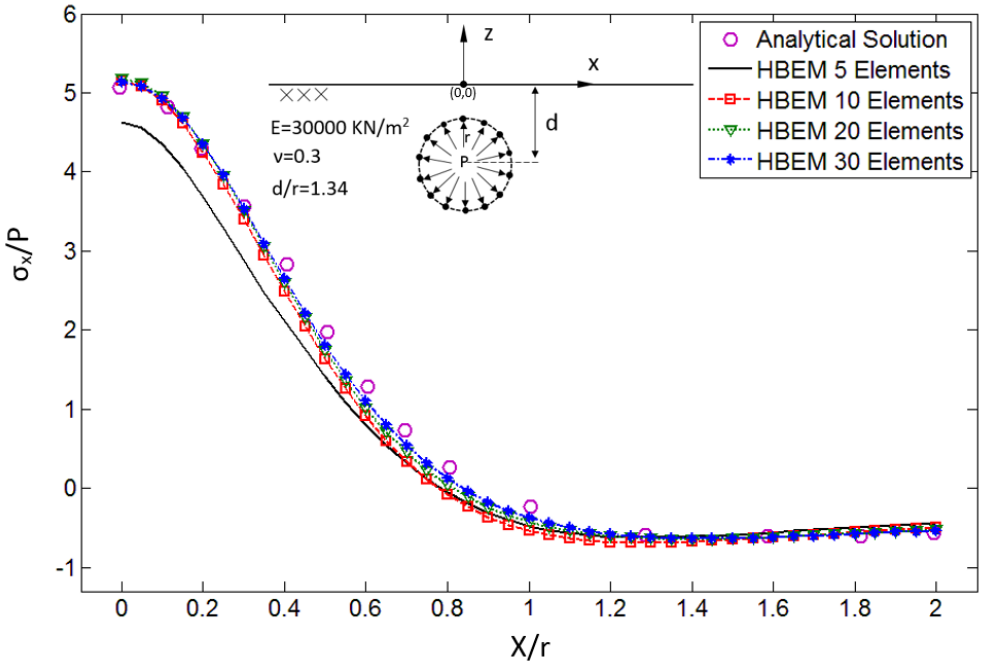

Fig. 9. Horizontal stress on the ground surface due to the presence of a circular cavity under pressure.

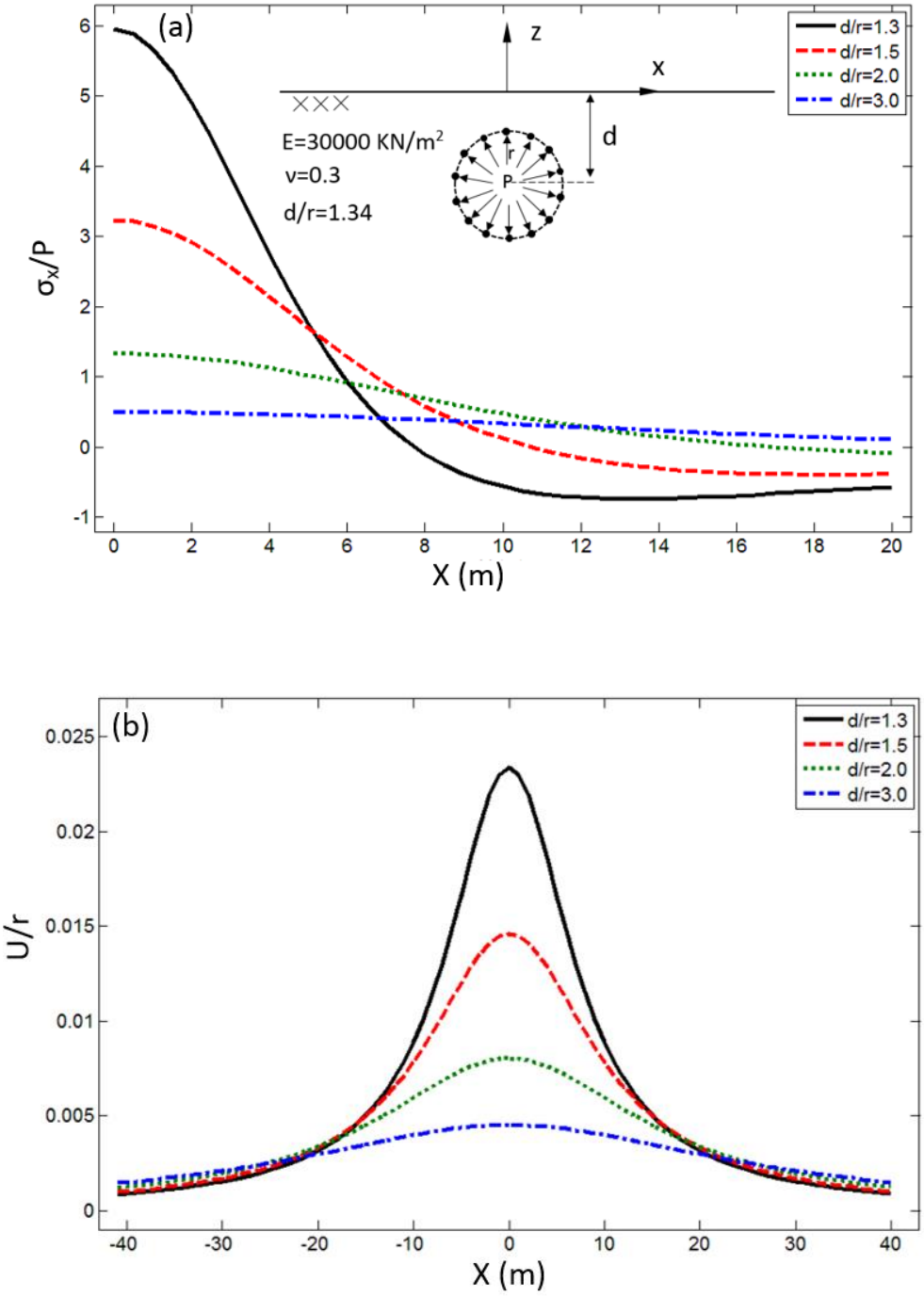

Fig. 10. Ground surface horizontal stresses (a) and vertical displacements (b) due to the presence of a circular cavity under pressure.

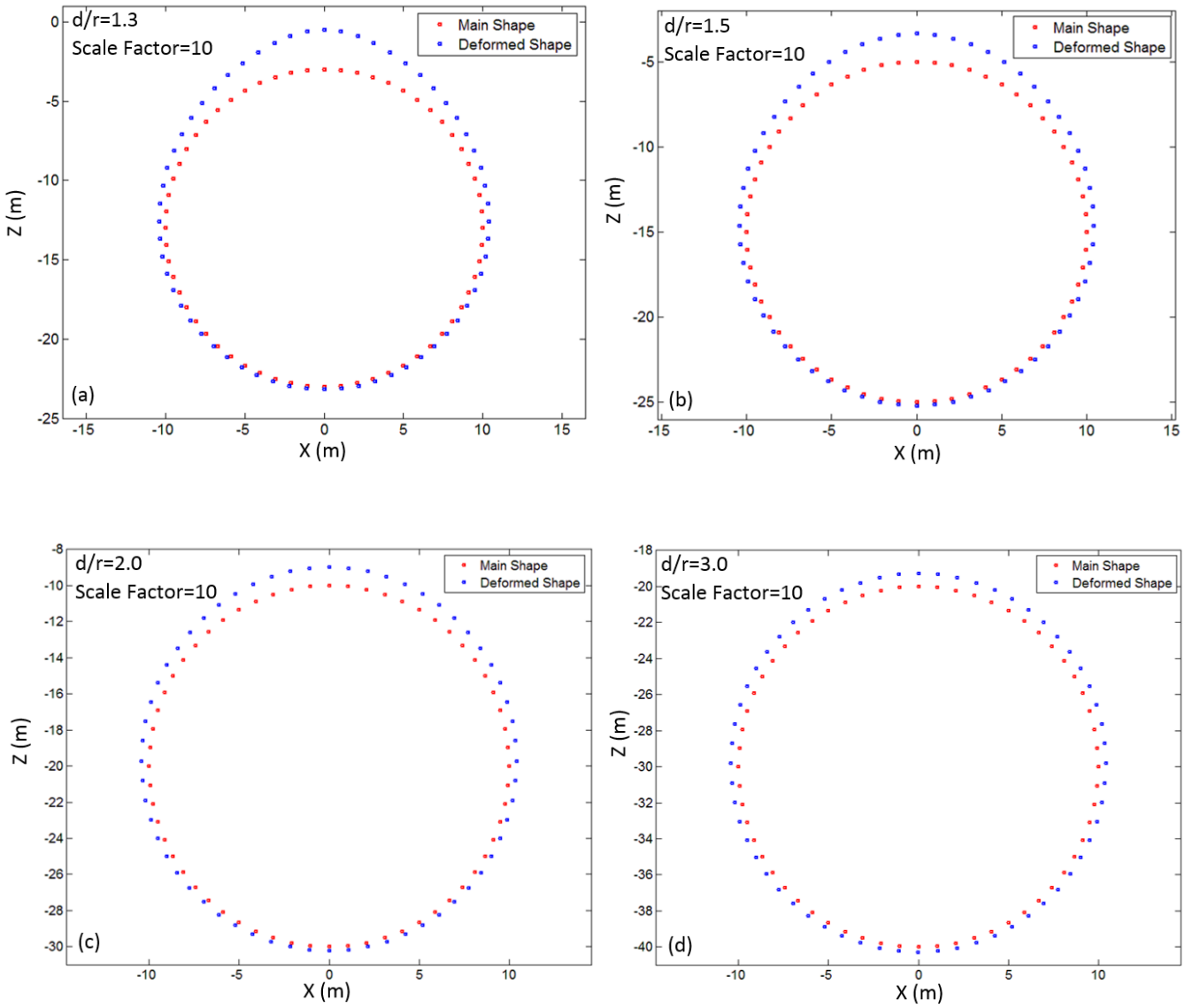

Fig. 11. Deformed shape versus the main shape of a shallow circular cavity (The displacement of the deformed shapes was scaled up 10 times for better visualization).

in Fig. 11 with a scale factor equal to 10. When the cavity is located at a shallower depth, the displacement in the top parts of the cavity grows more compared to that of the lower parts and by increasing the cavity depth the displacement becomes more uniform because of uniform confinement stresses. It is worth noting that for modeling this example only 30 half-plane elements were used. The same calculation can be done using ABAQUS finite element software with more than 700 domain elements [31] and with a full-plane boundary element code using 200 boundary elements [32].

7- Conclusion

In this paper, a new set of half-plane boundary element fundamental solutions for modeling semi-infinite geophysical problems was presented. In this regard, Papkovitch and Green's functions for a half-plane two-dimensional elastostatic space were introduced. Green's second identity was used as a tool for satisfying stress-free boundary conditions along the ground surface. The fundamental solutions were then obtained in two different types of loading. In the first case, displacement and traction fundamental solutions were obtained when the point load acts in the direction of the z-axis. In the second case,

the solutions when the point load acts in the direction of the x-axis were presented. These two sets of solutions provide a complete set of fundamental solutions required for a half-plane boundary element analysis.

The accuracy and efficiency of the half-plane solutions were evaluated by solving four classic examples. As the first set of examples, the ground surface vertical and horizontal displacements were evaluated indicating that the displacement set of half-plane fundamental solutions is correct and accurate. In the second set of examples, for testing the traction fundamental solutions, a shallow circular cavity under pressure embedded in a semi-infinite space was considered and the results for horizontal stresses on the ground surface were compared to an available analytical solution. The results again showed that the traction fundamental solutions work well for a boundary element analysis. All of these examples were solved only by a small number of boundary elements showing the power of boundary element analysis for solving half-plane problems.

The use of half-plane boundary element fundamental solutions does not introduce any special difficulties. All procedures including discretization, method of integration, solution of singularities, and calculation are the same as full-plane boundary element analysis. The discretization is only done for the boundaries of the model inside the loaded zone and also, the requirement to define artificial boundaries completely vanishes. These features reduce the computational time and calculation efforts which make the half-plane boundary element analysis a reliable solution for engineering problems.

References

[1] K.J. Bathe, Finite Element Procedures, 1st Ed., PRENTICE HALL, New Jersey, 1996.

[2] R.j. LeVeque, Finite Difference Methods for Ordinary and Partial Differential Equations (steady-state and time-dependent problems), First ed., Society for Industrial Applied Mathematics (Siam). Philadelphia, 2007.

[3] T.G. Sitharam, I.V.V. Kumar, Non-linear analysis of geotechnical problems using coupled finite and infinite elements, Geotechnical and Geological Engineering 16 (1998) 129-149.

[4] C.A. Brebbia, J. Dominguez, Boundary Elements An Introductory Course, 2 ed., Mechanic Publication, Boston, 1992.

[5] J.T. Katsikadelis, Boundary Elements Theory and Applications, 1 ed., Elsevier, Boston, 2002.

[6] M. Panji, B. Ansari, Modeling pressure pipe embedded in two-layer soil by a half-plane BEM, Computers and Geotechnics, 81 (2017) 360-367.

[7] C.A. Brebbia, M.H. Aliabadi, Adaptive Finite and Boundary Element Methods, 1 ed., WIT Press, 1993.

[8] C.A. Brebbia, D. Nardini, Dynamic analysis in solid mechanics by an alternative boundary element procedure, Engineering Analysis with Boundary Elements, 24(8) (2000) 513-518.

[9] B. Xiao, J.P. Carter, Boundary element analysis of anisotropic rock masses, Engineering Analysis with Boundary Elements, 11 (1993) 293–303.

[10] M. Panji, M.J. Asgari, S.h. Tavousi-Tafreshi, Evaluation of effective parameters on the underground tunnel stability using BEM, Journal of Structural Engineering and Geo-Techniques, 1 (2011) 29–37.

[11] M. Panji, H. Koohsari, M. Adampira, H. Alielahi, M.J. Asgari, Analyzing stability of shallow tunnels subjected to eccentric loads by a BEM approach, Journal of Rock Mechanics and Geotechnical Engineering, 8 (2016) 480–488.

[12] J. Boussinesq, Applications des Potentiels a` l'e´tude de l'e´quilibre et du mouvement des solids e´lastiques, 1 ed., Gauthier-Villars, Paris, 1885.

[13] V. Cerutti, Ricerche intorno all'equilibrio dei elastici isotropi, Mem. Della. Acc. dei Lin, 13 (1882) 81–123.

[14] E. Melan, Der spannungszustand der durch eine einzelkraft in innern beanspruchten halbscheibe, Applied Mathematics and Mechanics 12 (1932) 343-346.

[15] J.C.F. Telles, C.A. Brebbia, Boundary element solution for half-plane problems, International Journal of Solids and Structures, 12 (1980) 1149–1158.

[16] G.W. Ye, T. Sawada, Some numerical properties of boundary element analysis using half-plane fundamental solutions in 2-d elastostatics, Computational Mechanics 4(1989) 161-164.

[17] P.C. Dumir, A.K. Mehta, Boundary element solution for elastic orthotropic half-plane problems, Computers & Structures 26 (1987) 431–438.

[18] E. Pan, C.S. Chen, B. Amadei, A B EM formulation for anisotropic half-plane problems, Engineering Analysis with Boundary Elements, 20 (1997) 185-195.

[19] E. Pan, W. Chen, Static Green Functions in Anisotropic Media, 1st Ed., Cambridge University Press, London, 2015.

[20] C.Y. Dong, S.H. Lo, Boundary element analysis of an elastic half-plane containing nano-inhomogeneities, Journal of Materials Science 73 (2013) 33-40.

[21] R.D. Mindlin, Force at a point in the interior of a semi-infinite solid, Journal of Physics, 7 (1936) 195-202.

[22] B. John, J.R. Cheatham, The Use of Boussinesq-Papkovitch Stress Functions To Determine The Stresses Around The Bottom of a Cylindrical Cavity, Houston, Texas, 1960.

[23] C.E. Weatherburn, Advanced Vector Analysis, 1 ed., Bell's Mathematical Series, London, 1960.

[24] J. Cantarella, D. DeTurck, H. Gluck, Vector Calculus and the Topology of Domains in 3-Space, The American Mathematical Monthly, 109 (2002) 409–442.

[25] H.G. Poulos, E.H. Davis, Elastic Solutions for Soil and Rocks, 1st Ed., John Wiley and Sons, New York, 1974.

[26] N. Liu, A.E. Jeffers, A geometrically exact isogeometric Kirchhoff plate: Feature-preserving automatic meshing and C1 rational triangular Bézier spline discretizations, International Journal for Numerical Methods in Engineering, 115 (2018) 395-409.

[27] N. Liu, A.E. Jeffers, Rational Bézier Triangles for the Analysis of Isogeometric Higher-Order Gradient Damage

Models, in: 13th World Congress on Computational Mechanics (WCCM XIII) and 2nd Pan American Congress on Computational Mechanics (PANACM II), New York City, NY, USA, 2018.

[28] N. Liu, Non-Uniform Rational B-Splines and Rational Bezier Triangles for Isogeometric Analysis of Structural Applications, University of Michigan, 2018.

[29] R.L. Burden, J.D. Faires, Numerical Analysis, 9 ed., ROOKS/COLE CENGAGE learning, Boston, 2011.

[30] G.B. Jeffry, Plane Stress and Plane strain in bipolar coordinates, Philosophical Transactions of the Royal Society, 221 (1921) 265-293.

[31] M. Karakouzian, M. Karami, M. Nazari-Sharabian, S. Ahmed, Flow-Induced Stresses and Displacements in Jointed Concrete Pipes Installed by Pipe Jacking Method, Fluids, 4(34) (2019) 1-13.

[32] S. Parvanova, P. Dineva, Transient response analysis of anisotropic solids with nano-cavities by BEM. ZAMM, Journal of Applied Mathematics and Mechanics, 101(4) (2020) 1-19.

Appendix A

Required functions when point load ($p_z = 1$) is acted in the direction of the z-axis:

$$A_1(x,z) = -\frac{1}{\mu K}\left[\frac{x-\alpha}{r^2} + \frac{(3-4\nu)(x-\alpha)}{r'^2} + \frac{4\beta(x-\alpha)(z+\beta)}{r'^4}\right]$$

$$A_2(x,z) = \frac{1}{\mu K}\left[-4(1-\nu)(1-2\nu)\tan^{-1}\left(\frac{z+\beta}{x-\alpha}\right) + \beta\left(\frac{x-\alpha}{r^2} + \frac{(3-4\nu)(x-\alpha)}{r'^2}\right)\right]$$

$$A_3(x,z) = -\frac{1}{\mu K}\left[\ln r + (3-4\nu)\ln r' - \frac{2\beta(z+\beta)}{r'^2}\right]$$

$$A_4(x,z) = -\frac{1}{\mu K}\left[\frac{z-\beta}{r^2} + \frac{(3-4\nu)(z+\beta)}{r'^2} - \frac{2\beta\left[(x-\alpha)^2-(z+\beta)^2\right]}{r'^4}\right]$$

$$A_5(x,z) = \frac{1}{\mu K}\left[-4(1-\nu)(1-2\nu)\ln r' + \beta\left(\frac{z-\beta}{r^2} + \frac{(3-4\nu)(z+\beta)}{r'^2}\right)\right]$$

$$A_6(x,z) = -\frac{1}{\mu K}\left[\begin{array}{l}\dfrac{(z-\beta)^2-(x-\alpha)^2}{r^4} + \dfrac{(3-4\nu)\left[(z+\beta)^2-(x-\alpha)^2\right]}{r'^4} \\ + \dfrac{4\beta(z+\beta)\left[(z+\beta)^2-3(x-\alpha)^2\right]}{r'^6}\end{array}\right] \qquad \text{Eq. (A.1)}$$

$$A_7(x,z) = \frac{1}{\mu K}\left[\begin{array}{l}4(1-\nu)(1-2\nu)\dfrac{z+\beta}{r'^2} \\ +\beta\left(\dfrac{(z-\beta)^2-(x-\alpha)^2}{r^4} + \dfrac{(3-4\nu)\left[(z+\beta)^2-(x-\alpha)^2\right]}{r'^4}\right)\end{array}\right]$$

$$A_8(x,z) = -\frac{1}{\mu K}\left[\begin{array}{l}\dfrac{-2(x-\alpha)(z-\beta)}{r^4} - \dfrac{2(3-4\nu)(x-\alpha)(z+\beta)}{r'^4} \\ + \dfrac{4\beta(x-\alpha)\left[(x-\alpha)^2-3(z+\beta)^2\right]}{r'^6}\end{array}\right]$$

$$A_9(x,z) = \frac{1}{\mu K}\left[\begin{array}{l}-4(1-\nu)(1-2\nu)\dfrac{x-\alpha}{r'^2} \\ -2\beta(x-\alpha)\left(\dfrac{z-\beta}{r^4} + \dfrac{(3-4\nu)(z+\beta)}{r'^4}\right)\end{array}\right]$$

Required functions when unit point load ($p_x = 1$) is acted in the direction of the x-axis:

$$B_1(x,z) = -\frac{1}{\mu K}\left[\ln r + \ln r'\right]$$

$$B_2(x,z) = -\frac{(x-\alpha)}{\mu K}\left[\frac{1}{r^2} + \frac{1}{r'^2}\right]$$

$$B_3(x,z) = \frac{2}{\mu K}\left[-\frac{\beta\left((z+\beta)^2 - (x-\alpha)^2\right)}{r'^4} - \left(\frac{\lambda(1-2\nu)}{\mu} - 1\right)\frac{z+\beta}{r'^2}\right]$$

$$B_4(x,z) = \frac{2(1-2\nu)}{\mu K}\left[\frac{\beta(z+\beta)}{r'^2} - \left(\frac{\lambda(1-2\nu)}{\mu} - 1\right)\ln r'\right]$$

$$B_5(x,z) = \frac{2}{\mu K}\left[-\frac{\beta(x-\alpha)}{r'^2} + \left(\frac{\lambda(1-2\nu)}{\mu} - 1\right)\tan^{-1}\left(\frac{z+\beta}{x-\alpha}\right)\right]$$

$$B_6(x,z) = -\frac{1}{\mu K}\left[\frac{z-\beta}{r^2} + \frac{z+\beta}{r'^2}\right]$$

$$B_7(x,z) = \frac{2}{\mu K}\left[\frac{2\beta(x-\alpha)(z+\beta)}{r'^4} + \left(\frac{\lambda(1-2\nu)}{\mu} - 1\right)\frac{x-\alpha}{r'^2}\right]$$

$$B_8(x,z) = \frac{2(1-2\nu)}{\mu K}\left[-\frac{\beta(x-\alpha)}{r'^2} + \left(\frac{\lambda(1-2\nu)}{\mu} - 1\right)\tan^{-1}\left(\frac{z+\beta}{x-\alpha}\right)\right]$$

$$B_9(x,z) = -\frac{1}{\mu K}\left[\frac{(z-\beta)^2 - (x-\alpha)^2}{r^4} + \frac{(z+\beta)^2 - (x-\alpha)^2}{r'^4}\right] \qquad \text{Eq. (A.2)}$$

$$B_{10}(x,z) = \frac{4(x-\alpha)}{\mu K}\left[\frac{\beta\left(3(z+\beta)^2 - (x-\alpha)^2\right)}{r'^6} + \left(\frac{\lambda(1-2\nu)}{\mu} - 1\right)\frac{z+\beta}{r'^4}\right]$$

$$B_{11}(x,z) = \frac{2(1-2\nu)}{\mu K}\left[-\frac{2\beta(x-\alpha)(z+\beta)}{r'^4} - \left(\frac{\lambda(1-2\nu)}{\mu} - 1\right)\frac{x-\alpha}{r'^2}\right]$$

$$B_{12}(x,z) = \frac{2(x-\alpha)}{\mu K}\left[\frac{z-\beta}{r^4} + \frac{z+\beta}{r'^4}\right]$$

$$B_{13}(x,z) = \frac{2}{\mu K}\left[-\frac{2\beta(z+\beta)\left(3(x-\alpha)^2 - (z+\beta)^2\right)}{r'^6} - \left(\frac{\lambda(1-2\nu)}{\mu} - 1\right)\frac{(x-\alpha)^2 - (z+\beta)^2}{r'^4}\right]$$

$$B_{14}(x,z) = \frac{2(1-2\nu)}{\mu K}\left[\frac{\beta\left((x-\alpha)^2 - (z+\beta)^2\right)}{r'^4} - \left(\frac{\lambda(1-2\nu)}{\mu} - 1\right)\frac{z+\beta}{r'^2}\right]$$

In all the above expressions, (α, β) is the coordinate of the source point, (x, y) is the coordinate of the field point, μ and ν are the shear modulus, and Poisson's ratio, respectively, and $r = \sqrt{(x-\alpha)^2 + (z-\beta)^2}$ and $r' = \sqrt{(x-\alpha)^2 + (z+\beta)^2}$ are the distance of the source point and its image from the field point, respectively.

Appendix B

Telles and Brebbia [15] presented a set of half-plane boundary element fundamental solutions. However, the traction set of their solutions doesn't completely support the stress-free condition of the ground surface.

The complementary part of the traction solutions have been presented as follows:

$$\sigma_{122}^{c} = -\frac{1}{4\pi(1-\nu)}\left\{\frac{(3\bar{x}+c)(1-2\nu)}{R^2} + \frac{2\left[\left(2c\bar{x}+r_2^2\right)R_1 - 2\bar{x}R_1^2(1-2\nu)\right]}{R^4} - \frac{16c\bar{x}R_1 r_2^2}{R^6}\right\} \quad \text{Eq. (B.1)}$$

Where all parameters are available in the Telles and Brebbia [15]. When the field point is located on the ground surface, $\bar{x} = 0$, $c = \beta$, $R_1 = -\beta$ and $r_2 = x - \alpha$; therefore:

$$\sigma_{122}^{c} = -\frac{\beta}{4\pi(1-\nu)R^2}\left\{1-2\nu-\frac{2(x-\alpha)^2}{R^2}\right\} \quad \text{Eq. (B.2)}$$

The traction component on the surface can be obtained as follows:

$$p_{22}^{c} = \frac{\beta}{4\pi(1-\nu)R^2}\left\{1-2\nu-\frac{2(x-\alpha)^2}{R^2}\right\} \quad \text{Eq. (B.3)}$$

For the ground surface, the Kelvin part of the solutions which must be added to the complementary part is available in Brebbia and Dominguez [4] as follows:

$$p_{22} = -\frac{\beta}{4\pi(1-\nu)R^2}\left\{1-2\nu+\frac{2(x-\alpha)^2}{R^2}\right\} \quad \text{Eq. (B.4)}$$

The sum of p_{22}^{c} and p_{22} is not equal to zero showing that the σ_{122}^{c} does not support the ground surface stress-free condition properly.

HOW TO CITE THIS ARTICLE

B. Ansari, A. R. Firoozfar, Half-Plane Boundary Element Fundamental Solutions and Body Force, AUT J. Civil Eng., 5(4) (2021) 625-642.

DOI: 10.22060/ajce.2022.19447.5732